Analytica Chimica Acta 1278 (2023) 341725

Contents lists available at ScienceDirect

Analytica Chimica Acta

journal homepage: www.elsevier.com/locate/aca

Unravelling dispersion forces in liquid-phase enantioseparation. Part I: Impact of ferrocenyl versus phenyl groups

Barbara Sechi [a,1], Alessandro Dessì [a,1], Roberto Dallocchio [a,1], Nutsa Tsetskhladze [b], Bezhan Chankvetadze [b], Mireia Pérez-Baeza [c], Sergio Cossu [d], Giorgi Jibuti [b], Victor Mamane [e,**], Paola Peluso [a,*]

[a] Istituto di Chimica Biomolecolare ICB-CNR, Sede Secondaria di Sassari, Traversa La Crucca 3, Regione Baldinca, Li Punti, 07100, Sassari, Italy
[b] Institute of Physical and Analytical Chemistry, School of Exact and Natural Sciences, Tbilisi State University, Chavchavadze Ave 3, 0179, Tbilisi, Georgia
[c] Departamento de Química Analítica, Universitat de València, Burjassot, València, Spain
[d] Dipartimento di Scienze Molecolari e Nanosistemi DSMN, Università Ca' Foscari Venezia, Via Torino 155, I-30172, Mestre Venezia, Italy
[e] Institut de Chimie de Strasbourg, UMR, CNRS 7177, Equipe LASYROC, 1 Rue Blaise Pascal, 67008, Strasbourg Cedex, France

HIGHLIGHTS

- Enantioseparations on coated and immobilized polysaccharide-based selectors.
- Chiral analytes featuring extended π-electron clouds.
- Computational analysis is used to unravel enantioseparation mechanism.
- Dispersion forces may reasonably contribute to enantioselective recognition.

GRAPHICAL ABSTRACT

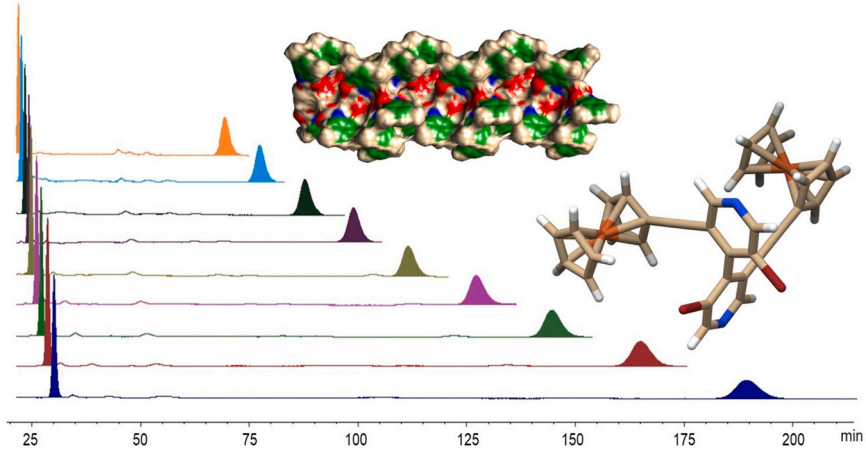

ARTICLE INFO

Keywords:
Enantioseparation
Ferrocene
Molecular modeling
Noncovalent interactions
Polysaccharide-based chiral stationary phases

ABSTRACT

Background: Highly ordered chiral secondary structures as well as multiple (tunable) recognition sites are the keys to success of polysaccharide carbamate-based chiral selectors in enantioseparation science. Hydrogen bonds (HBs), dipole-dipole, and π-π interactions are classically considered the most frequent noncovalent interactions underlying enantioselective recognition with these chiral selectors. Very recently, halogen, chalcogen and π-hole bonds were also identified as interactions working in polysaccharide carbamate-based selectors to promote

* Corresponding author.
** Corresponding author.
E-mail addresses: vmamane@unistra.fr (V. Mamane), paola.peluso@cnr.it (P. Peluso).
[1] These authors contributed equally to this work.

https://doi.org/10.1016/j.aca.2023.341725
Received 8 June 2023; Received in revised form 12 August 2023; Accepted 14 August 2023
Available online 17 August 2023

enantiomer distinction. On the contrary, the function of dispersion interactions in this field was not explored so far.

Results: The enantioseparation of chiral ferrocenes featuring chiral axis or chiral plane as stereogenic elements was performed by comparing five polysaccharide carbamate-based chiral columns, with the aim to identify enantioseparation outcomes that could be reasonably determined by dispersion forces, making available a reliable experimental data set for future theoretical studies to confirm the heuristic hypothesis. The effects of mobile phase polarity and temperature on the enantioseparation were considered, and potential recognition sites on analytes and selectors were evaluated by electrostatic potential (*V*) analysis and molecular dynamics (MD). In this first part, the enantioseparation of 3,3′-dibromo-5,5′-bis-ferrocenylethynyl-4,4′-bipyridine bearing two ferrocenylethynyl units linked to an axially chiral core was performed and compared to that of the analyte featuring the same structural motif with two phenyl groups in place of the ferrocenyl moieties. The results of this study showed the superiority of the ferrocenyl compared to the phenyl group, as a structural element favouring enantiodifferentiation.

Significance and novelty: Even if dispersion (London) forces have been envisaged acting in liquid-phase enantioseparations, focused studies to explore possible contributions of dispersion forces with polysaccharide carbamate-based selectors are practically missing. This study allowed us to collect experimental information that support the involvement of dispersion forces as contributors to liquid-phase enantioseparation, paving the way to a new picture in this field.

1. Introduction

Polysaccharide carbamate-based chiral stationary phases (CSPs) are the most versatile tools that analytical scientists have at disposal today to separate the enantiomers of a chiral compound [1]. Versatility and high performances of these chiral selectors are mainly due to their highly ordered chiral secondary structure as well as to the presence of multiple recognition sites. In this chiral environment, mobile phase polarity and temperature may tune the strength of noncovalent interactions occurring between selector and analyte enantiomers. In principle, a huge number of noncovalent interactions of various kind can underlie adsorption and enantioselective recognition on polysaccharide carbamate-based selectors allowing for successful enantioseparation of a large series of chiral compounds. This aspect has represented the key to success of polysaccharide carbamate-based polymers in enantioseparation science, also making them suitable to study mechanisms underlying enantioseparation at molecular level by integrating experimental and theoretical analysis [2]. This is still an urgent issue in enantioseparation science because the structural complexity of polysaccharide derivatives makes the understanding of their functioning at molecular level rather challenging.

Hydrogen bonds (HBs), dipole-dipole, and π-π interactions are classically considered the most frequent intermolecular noncovalent interactions underlying enantioselective recognition with polysaccharide carbamate-based selectors. Intramolecular HBs within both polysaccharide-based selectors [2,3] and analytes [4] may significantly contribute to enantioselective recognition. Very recently, halogen [5], chalcogen and π-hole bonds [6] were also identified as interactions working in polysaccharide carbamate-based selectors to promote enantiomer distinction. On the contrary, dispersion interactions still represent an open issue in this field, and no study clearly profiled and quantified these forces in chromatography enantioseparation so far. It is evident that there is a gap of knowledge that should not be ignored. On one hand, it is possible that a scientific issue does not occur if there exists no approach to answer it unambiguously. Furthermore, if HB may act as dominant noncovalent interaction in a molecular system, it is classically thought that charge transfer and/or electrostatic effects are the main occurring components [7]. On the other hand, another picture may be envisaged given that dispersion energy contribution to noncovalent interactions such as HB, and even more π-π interactions, may be not negligible, and dispersion forces can greatly contribute to binding and recognition involving extended molecular surfaces [8].

Given this context, in this study the enantioseparation of chiral ferrocenes featuring chiral axis or chiral plane as stereogenic elements and extended π-electron clouds was considered with the following aims: *a*) exploring the possibility of unusual chromatographic behaviours which could be reasonably ascribed to dispersion forces; *b*) profiling reliable benchmark experimental data set suitable to investigate dispersion-based mechanisms by theoretical and computational analysis, confirming the heuristic hypothesis inspiring this experimental study. In this regard, it is worth mentioning that, so far, the functioning of dispersion forces has been verified by reliable real-life experimental data in a limited number of cases, especially in solution, and most investigations have been conducted either for nonconventional systems or employed only theoretical reference data, often performed in the vacuum [9]. Moreover, currently available dispersion-corrected theoretical approaches may overestimate dispersion contribution in solution [10].

In this first part, the enantioseparation of the 3,3′-dibromo-5,5′-bis-ferrocenylethynyl-4,4′-bipyridine **1** (Fig. 1) bearing two ferrocenylethynyl units linked to an axially chiral core was considered with the aim to study the impact of ferrocene on the enantioseparation process. For this purpose, a second analyte, the 3,3′-dibromo-5,5′-bis-phenylethynyl-4,4′-bipyridine **2** (Fig. 1), featuring the same structural motif but with two phenyl groups in place of the ferrocenyl moieties, was also evaluated as reference for comparison. Five polysaccharide phenylcarbamate-based chiral columns (Lux Cellulose-1, i-Cellulose-5, Amylose-1, i-Amylose-1, and i-Amylose-3) (Table S1, Supplementary data) were used and compared in this study. Given that noncovalent interactions between analyte enantiomers and selector largely depend on the structures of selector and chiral analyte, and on mobile phase polarity, possible recognition sites on both analytes and selectors were evaluated by electrostatic potential (*V*) analysis and molecular dynamics (MD), and the effects of introducing methanol (MeOH) in the mobile phase was also considered. Finally, the effect of temperature on retention and selectivity was evaluated, and overall thermodynamics parameters associated with the analyte adsorption onto the CSP surface were derived from van't Hoff plots.

2. Materials and methods

2.1. Reagents and chemicals

Compounds **1** and **2** were prepared and characterized as previously reported [11]. HPLC grade *n*-hexane, MeOH, and propan-2-ol (2-PrOH), were purchased from Sigma-Aldrich (Taufkirchen, Germany).

2.2. Chromatography

An Agilent Technologies (Waldbronn, Germany) 1100 Series HPLC system (high-pressure binary gradient system, a diode-array detector operating at multiple wavelengths [220, 254, 280, 360 nm], and a programmable autosampler with a 20 μl loop) was employed. Data

acquisition and analyses were carried out with Agilent Technologies ChemStation Version B.04.03 chromatographic data software. The UV absorbance is reported as milliabsorbance units (mAU). Lux Cellulose-1 [cellulose *tris*(3,5-dimethylphenylcarbamate)], Lux i-Cellulose-5 [cellulose *tris*(3,5-dichlorophenylcarbamate)], Lux Amylose-1 and Lux i-Amylose-1 [amylose *tris*(3,5-dimethylphenylcarbamate)], and Lux i-Amylose-3 [amylose *tris*(3-chloro-5-methylphenylcarbamate)] (5 μm) (Phenomenex Inc., Torrance, CA, USA) (Table S1, Supplementary data) were used as chiral columns (250 × 4.6 mm). Analyses were performed in isocratic mode at 25 °C, if not indicated otherwise. The flow rate was set at 0.8 ml/min. Dead time (t_0) was measured by injection of tri-*tert*-butylbenzene (Sigma-Aldrich) as a non-retained compound [12]. For compounds **1** and **2**, the enantiomer elution order (EEO) was determined by injecting enantiomers of known absolute configuration, (*P*) or (*M*) [11]. The van 't Hoff experiments were conducted at 5, 10, 15, 20, 25, 30, 35, 40, and 45 °C by using a thermostat jacket equipped with a RE104 Lauda circulating water bath (Lauda, Königshofen, Germany) (resolution 0.1 °C; accuracy ±0.4 °C; temperature control ±0.02 °C). When the temperature was changed, the column was allowed to equilibrate for 1 h before injecting the samples. Thermodynamics parameters were derived from the slopes and the intercepts of the van't Hoff plots by linear regression analysis (see Supplementary data for details). Statgraphics Centurion 18 (Statpoint Technologies, Inc., Warrenton, VA, USA) was used for all linear regression analyses.

2.3. Computations

V extrema (maxima and minima) on the molecular electron density isosurfaces ($V_{S,max}$ and $V_{S,min}$) (au, electrons/Bohr) were calculated by using Gaussian 09 (Wallingford, CT, USA) [13], at the density-functional theory (DFT) level using the B3LYP functional and the def2-TZVPP basis set. Search for the exact location of $V_{S,max}$ and $V_{S,min}$ was made through the Multiwfn code [14] and through its module enabling quantitative analyses of molecular surfaces (isovalue 0.002 a. u.) [15]. The .wfn files were obtained through the Gaussian 09 package. Details for MD are reported in the Supplementary data.

3. Results and discussion

3.1. Dispersion forces

The aim of this section is to describe dispersion forces and the features that make them of interest in chromatography and enantioseparation science. Dispersion or London forces are defined as "*attractive forces between apolar molecules, due to their mutual polarizability. They are also components of the forces between polar molecules.*" [16]. The London dispersion term is referred to the attractive component of the van der Waals interactions, originating from an electron correlation effect occurring between atoms or molecules in which dipoles can be induced instantaneously [17]. As summarized by Grimme, dispersion interactions are *a*) ubiquitous and always attractive, *b*) per atom-pair interaction on the order of a factor 100 weaker than covalent ones, *c*) long-ranged, and *d*) additive in character [18]. This last feature is a key point. On one hand, for long time dispersion forces were considered weak and used almost exclusively to rationalize the greater stability of branched over linear alkanes, neglecting them as stabilizing interactions in other chemical contexts [17]. On the contrary, more recently, the importance of dispersion forces has been fully recognized in several applicative fields [19]. Indeed, being ubiquitous, attractive, and additive, dispersion forces can stabilize medium- and large-sized (polarizable) molecular systems, contributing to increase interaction energy between large-sized hydrocarbon fragments. Dispersion forces oppose to repulsion mechanisms determined by the steric hindrance between spatially close-lying functional groups [9,17], in other words turning 'steric repulsion' into 'steric attraction' [20]. The importance of London dispersion interactions in condensed matter is still an open issue, and the degree of their attenuation in solution is not properly understood so far [21,22]. Although these interactions are tendentially weakened in solution, they may persist in alkane-based solvents as well as in other several media [22,23]. Very recently, dispersion forces have been shown to play an important role in asymmetric catalysis, where small differences in transition states determine high degree of stereoselectivity [24,25].

3.2. Dispersion forces in liquid-phase chromatography

The possibility that dispersion forces may also act in liquid-phase chromatography was considered by Scott in the late 1970s ("*Where polar forces between the solute and each phase are weak, it is shown that dispersive interactions in the mobile phase are proportional to the density of the dispersing solvent* (i.e. *n*-heptane).") [26]. Experimental studies also considered the possibility of dispersion interactions in separation processes involving nonpolar stationary phases and analytes under reversed-phase elution conditions [27,28]. By using computer simulation and adsorption spectra to study the interaction between fullerenes and corannulene, Kubo *et al.* showed that the high retention of corannulene on a C_{70} bonded silica-monolithic column was effectively due to dipole-induced dipole interactions [29]. Later, the same group found that dipole-induced dipole interactions were dominant in the separation of saccharides using fullerene-bonded silica monolithic columns in liquid chromatography, observing that maltose, with the higher dipole moment, was more strongly retained compared to other disaccharides having lower dipole moment [30].

In 2011, West *et al.* reported the use of linear solvation energy relationships (LSER) to predict retention and the degree of separation between two enantiomers in the case of polysaccharide carbamate-based chiral stationary phases used in supercritical fluid chromatography [31]. This LSER model also comprised dispersion interactions through two

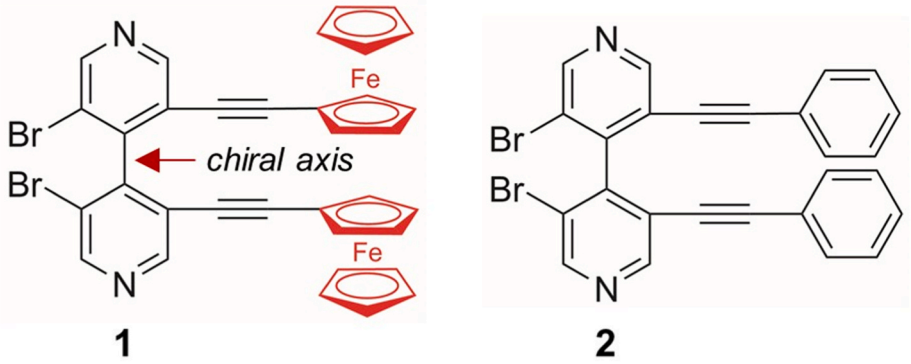

Fig. 1. Structures of chiral compounds **1** and **2**.

descriptors: *a*) *E*, reflecting polarizability contributions from n and π electrons, was used to describe London, Debye (dispersive and dipole-induced dipole), and π–π interactions; *b*) *V*, reflecting McGowan molecular volume and describing again London interactions, cavity effect or hydrophobic effect, and steric resistance to insertion in chiral cavities [32]. Thus, the model considered two structural features as possible sources of dispersion forces, namely *a*) n and π-electron systems, and *b*) large-sized frameworks. Despite this, studies focused on exploring dispersion interactions with polysaccharide-based selectors were not reported so far, and generic statements reported in the literature about dispersion interactions in enantioseparation science remain rather speculative in their character, lacking theoretical and experimental bases.

3.3. Structural features of compounds **1** and **2**

The choice of analytes **1** and **2** as test probes for dispersion interactions was based on the following points.

a) To design the dispersion probes, ferrocenyl and phenyl groups were introduced in a 4,4′-bipyridyl scaffold based on the results of our previous studies. Indeed, we showed that, for atropisomeric 4,4′-bipyridines, the enantioseparation extent depends on the structural features of the substituents located at the 3,3′,5,5′ positions of the heteroaromatic scaffold, close to the chiral 4,4′-axis [33].
b) Ferrocene is an attractive structure as 'dispersion energy donor'. In this regard, Grimme remarked that the presence of large, electron-rich, and polarizable chemical groups in a molecular system as 'dispersion energy donors' can be used to energetically stabilize the system itself, and to orientate molecular recognition processes and chemical reactivity through dispersion forces [9]. Theoretically, it was demonstrated that dispersion interactions contribute to ligand-ligand interaction in ferrocene [34] and to stabilize ferrocene dimer [35]. Recently, dispersion forces were found to determine the conformational preferences in ferrocenes containing extended π-electronic clouds [36].
c) In general, dispersion was found to have the major role in π-π stacking interactions, the magnitude of these interactions being more size-dependent in aromatic systems than in saturated systems, and the strength of π-π interactions growing more quickly with an increasing size of the interacting partners [37]. For this reason, the comparison between ferrocenyl and phenyl, as distinctive substituents in compounds **1** and **2**, respectively, could be fruitful for the purpose. Indeed, although both **1** and **2** are characterized by extended π-electron systems formed by the pyridyl ring, the ethynyl linker, and the aromatic pendants, derivative **1** presents higher area and volume (594 Å^2, 581 Å^3) compared to the analogue **2** (433 Å^2, 427 Å^3) due to the presence of the large-sized ferrocenyl moieties in place of the phenyl groups. The ferrocenyl moieties present a three-dimensional sandwich-like spatial arrangement, the ferrocene being considered a three-dimensional analogue of the flat benzene ring [38], with a cylindrical shape which may offer better possibility for filling hydrophobic cavities compared to the phenyl rings, and a more extended area for interactions. On this basis, despite a common 3,3′-dibromo-4,4′-bipyridine structure, compounds **1** and **2** appeared very different in term of overall geometry and electron charge density distribution, the ferrocenyl derivative resulting in a large-sized extended π-electron system, likely more polarizable, compared to the phenyl derivative **2.**
d) In compound **1**, the two ferrocenyl groups are not symmetrically distributed around the 4,4′-bipyridyl unit in the lowest energy conformation, as confirmed by X-ray diffraction analysis [11] and theoretical calculations (Table 1). Indeed, whereas one may expect that the ferrocenyl groups orientate far from the bipyridyl moiety because of steric repulsion, both metallocene units are in front of the closest pyridyl ring, with ferrocenyl (A) – pyridyl (B) and ferrocenyl (B) – pyridyl (A) intramolecular distances ranging from 2.8 to 4.1 Å [11]. This observation may be interpreted as turning of an expected steric repulsion into attraction because of the inherent capability of ferrocene as 'dispersion donor'. On the contrary, in compound **2**, the two phenyl groups are symmetrically distributed around the heteroaromatic scaffold with a divergent orientation.
e) Using potential 'dispersion energy donors' containing an extended π-electronic cloud presents at least two practical advantages compared to alkyl hydrocarbon frameworks: *i*) higher UV-based detectability of the chromophore system, and *ii*) higher selectivity associated to the enantiophore system. In this regard, to explore and compare the interaction capability of **1** and **2**, in terms of electron charge density distribution on the main interaction sites of both compounds, the *V* extrema were calculated at DFT level of theory (B3LYP/def2TZVPP) and mapped on 0.002 au electron density isosurfaces (Table 1). It is worth mentioning that, given a molecule, the $V(\mathbf{r})$ at each point $\mathbf{r}$ in the surrounding space, is created by each nucleus (first positive term) and electron (second negative term) of the molecule and given by equation (1)

$$V(\mathrm{r}) = \sum_A \frac{Z_A}{R_A - \mathbf{r}} - \int \frac{\rho(\mathbf{r})d\mathbf{r}'}{|\mathbf{r}' - \mathbf{r}|} \quad (1)$$

where Z_A is the charge on nucleus A located at R_A, and $\rho(\mathbf{r})$ is the electron density function [39]. Thus, the sign of *V* may be positive or negative depending on the dominant contribution, which is positive and negative from nuclei and electrons, respectively. *V* is a real physical property, and the evaluation of its variations on a molecular electron density isosurface accounts for the shape of the molecule which is the sum of geometry and electronic distribution. On this basis, *V* analysis may give information on specific regions of the

Table 1
Calculated $V_{S,max}$ and $V_{S,min}$ (au) values on a 0.002 au electron density isosurface for the main possible interaction sites of compounds **1** and **2** (Gaussian 09, DFT/B3LYP/def2TZVPP). Color legend: Br, dark red; C, tan; Fe, orange; H, white; N, blue (Cp, Cyclopentadienyl; Ph, Phenyl).

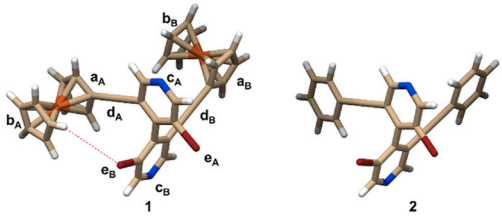

Descriptor	$V_{S,max}$	$V_{S,min}$
1		
Cp $\mathbf{a_A}$		−0.0184
Cp $\mathbf{a_B}$		−0.0190
Cp $\mathbf{b_A}$		−0.0222
Cp $\mathbf{b_B}$		−0.0230
N $\mathbf{c_B}$		−0.0606
N $\mathbf{c_A}$		−0.0604
C≡C $\mathbf{d_A}$		−0.0201
C≡C $\mathbf{d_B}$		−0.0274
Br $\mathbf{e_B}$	0.0348	
Br $\mathbf{e_B}$		−0.0178
Br $\mathbf{e_A}$	0.0330	
Br $\mathbf{e_A}$		−0.0201
2		
Ph		−0.0141
Br	0.0358	
Br		−0.0163
C≡C		−0.0225
N		−0.0586

molecules, such as lone pairs and π-clouds. The analysis of the *V* extrema (Table 1) of **1** and **2** showed that more negative $V_{S,min}$ values were calculated for compound **1** (-0.0606 au $\leq V_{S,min} \leq -0.0178$ au) compared to **2** (-0.0586 au $\leq V_{S,min} \leq -0.0141$ au) for the main nucleophilic recognition sites (N, C≡C, cyclopentadienyl (Cp) or phenyl (Ph), Br), thus the electron charge density on these sites was higher in the first case. Otherwise, the $V_{S,max}$ on bromine was more positive for compound **2** compared to **1**, thus bromine appeared as a better electrophile in **2**. For the latter compound, the *V* analysis confirmed the symmetric electron charge density distribution in respect of the two disubstituted pyridyl rings, emerging from the symmetric structure of the analyte. In this case, the $V_{S,min}$ values became less negative following the order N < C≡C < Br < Phenyl. On the contrary, in compound **1** the 3-bromo-5-ferrocenylethynyl-4--pyridyl framework (B) appeared more electron-rich ($V_{S,min}$: N < C≡C < Cp (**b**) < Cp (**a**) < Br) compared to the other 3′-bromo-5′-ferrocenylethynyl-4′-pyridyl framework pyridyl system (A) ($V_{S,min}$: N < Cp (**b**) < C≡C, Br < Cp (**a**)), this difference likely emerging from the proximity of ferrocenyl and pyridyl moieties in the most stable conformation, mutually affecting their *V* values due to intramolecular contacts [39]. Although both analytes could form HBs with the chiral selector through the pyridyl nitrogen atoms and the ethynyl π-clouds as HB acceptors as well as interactions involving their extended π-electron clouds, different electron charge density distributions and shapes were expected to result in different enantioseparation profiles and recognition mechanisms.

f) In a different perspective, it is also worth noting that the enantioseparation of chiral ferrocenes is of great interest because, despite the applicative importance of these compounds, few analytical studies focused on enantiorecognition mechanisms involving the ferrocenyl system which remained scarcely explored in enantioseparation science [38,40–42].

3.4. Polysaccharide tris(3,5-disubstitutedphenylcarbamates) as chiral selectors

Polysaccharide phenylcarbamate derivatives are characterized by a modular polymeric system where the polysaccharide backbone generates conformational chirality depending on the peculiar helical twist generated by specific glycosidic linkages in cellulose and amylose polymeric chains. The polymer backbone is functionalized with substituted (methyl groups and/or chlorine atoms) phenylcarbamate groups able to exert various noncovalent interactions [2,3]. The overall system characterizing polysaccharide-based selectors provides an extended surface to host the enantiomers of a chiral compound in the chiral cavities featuring the polymeric groove and containing various types of tunable polar and nonpolar recognition sites. In this regard, it is worth mentioning that 3,5-dialkylated aryl frameworks have proved to be very efficient as dispersion energy donors in asymmetric catalysis, contributing to dispersion interactions with nonpolar moieties in proximity [23,43,44]. Thus, among the polysaccharide-based chiral columns commercially available [1,3], we used in this study three 3,5-dimethylated columns based on cellulose (Lux Cellulose-1) and amylose (Lux Amylose-1 and i-Amylose-1) *tris*(3,5-disubstitutedcarbamates). Furthermore, two additional chlorinated chiral columns (i-Cellulose-5 and i-Amylose-3) were also considered with the aim to explore the impact of changing pendant group structure on selector performance toward analytes **1** and **2**. Indeed, the substituents of the phenylcarbamate pendant groups impact the performances of the corresponding polysaccharide derivatives as chiral selectors in terms of electron charge density of the carbamate moiety [1–3]. Thus, the useful descriptor *V* was again considered for comparing the electron charge density distribution on the carbamate moieties of different selectors, and *V* extrema on the carbonyl oxygen ($V_{S,min}$) and the amidic hydrogen ($V_{S,max}$) were calculated and compared (Table S1, Supplementary data) [5]. The substituents exert an opposite effect on the two main carbamate recognition sites (C=O and *N*–H) and, consequently, the electron charge density distribution on the carbonyl oxygen as nucleophile and the acidity of the amidic hydrogen as electrophile decreases (the $V_{S,min}$ becomes less negative) and increases (the $V_{S,max}$ becomes more positive) respectively, moving from 3,5-dimethyl- ($V_{S,min} = -0.0660$ au; $V_{S,max} = 0.0788$ au), to 3-chloro-5-methyl- (-0.0594 au; 0.0871 au) and 3,5-dichlorophenylcarbamates (-0.0561 au; 0.0950 au).

Moreover, by changing backbone and substituent type, the features of the interacting surface also change. Overtime, 3,5-disubstituted phenylcarbamates as pendant groups have proven to lend the corresponding chiral columns higher versatility toward several classes of chiral compounds, irrespective of substituent type. On the other hand, pendant groups can also determine the shape of the chiral cavities hosting the chiral analyte. To confirm this hypothesis at molecular level, in the beginning of this study, three amylose 4/3 left-handed helical phenylcarbamate-based nonamers (9-mer) featuring *a*) two methyl groups at the positions 3 and 5, *b*) one methyl group at the position 4, and *c*) two methyl groups at the positions 2 and 5 of the phenylcarbamate pendant groups, respectively, were built as virtual polymers, and the shape of their chiral cavities was explored by MD, carrying out 100 ns MD simulations, with the mixture *n*-hexane/2-PrOH 90:10 as explicit virtual solvent. The 9-mer structure, containing the terminal hydroxyl groups capped by adding methyl groups in place of the hydrogens, was modeled as reported in our previous studies [45]. This is one of the most used models for polysaccharide-based selectors along with the 12-mer oligomer, proposed by Okamoto et al. [46] in 2002 for the amylose *tris*(3,5-dimethylphenylcarbamate). In the last few years, 9-mer models of polysaccharide-based selectors showed good reliability for explaining the molecular bases of the enantioseparation by molecular modeling, and MD performed with this relatively simple strand provided results in agreement with the experiments in several cases [2]. In this regard, it is worth mentioning that a single alternative model consisting of multiple amylose *tris*(3,5-dimethylphenylcarbamate) polymer strands coated on an amorphous silica slab was reported so far [47], which was used to model a limited number of enantioseparations. On the other hand, the experimental benchmarks underlying the preparation of this very complex model appears rather arbitrary, also considering that no clear and unambiguous structural information about polysaccharide-based stationary phases were reported until now.

The results of the simulations performed in this study supported our hypothesis, and the three different substitution patterns profiled three different shapes for the corresponding chiral cavities (Fig. 2): *a*) *cup-shaped cavities* for the 3,5-disubstitution (A), *b*) *open-shaped cavities* for the 4-substitution (B), and *c*) *cavities made hindered* by the 2-methyl protruding inside the groove in the case of the 2,5-disubstitution (C). On this basis, while the 'open-shaped cavity' could be too large for small analytes and the 'hindered cavity' too small for large-sized analytes, the 'cup-shaped cavity' appeared geometrically more hospitable toward analytes of different size.

The MD simulations *a*) provided a rational explanation at molecular level for the higher versatility of polysaccharide *tris*(3,5-disubstitutedcarbamates) as chiral selectors in enantioseparation science, and *b*) confirmed the advantage of using chiral columns with adaptive 'cup-shaped cavities' featuring the extended polymeric surface.

3.5. Chromatographic screening with n-hexane/2-PrOH 90:10 v/v as mobile phase: impact of CSP structure

n-Hexane/2-PrOH 90:10 v/v was used as mobile phase to perform a chromatographic screening aiming at evaluating how changing chiral selector, in terms of backbone (amylose or cellulose) and substituents (methyl and/or chlorine) at the 3 and 5 positions of the pendant groups, impacted on the enantioseparation of compounds **1** and **2**. The main purpose of this screening was to confirm if, as expected, two different enantioseparation profiles could be observed for analytes **1** and **2**. The chromatographic results are summarized in Fig. 3 (for chromatographic

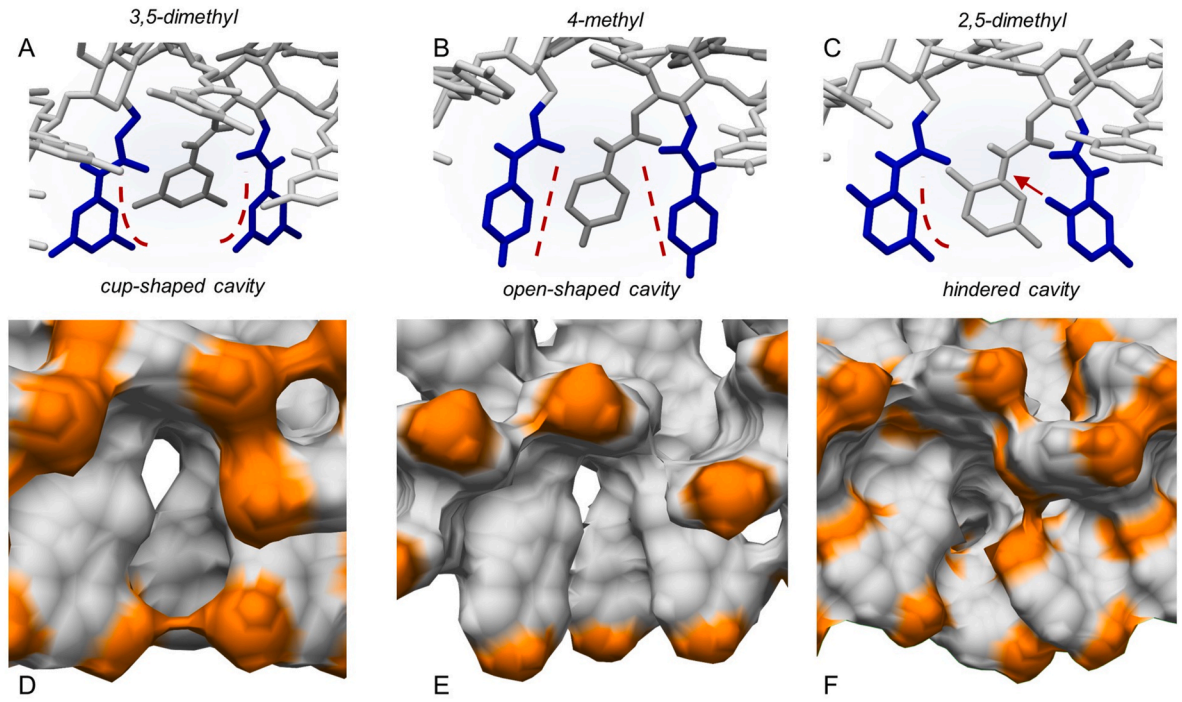

Fig. 2. Typical shapes of the chiral cavities into amylose carbamate-based chiral stationary phases modeled as drawing structures (A–C) and as electron density surfaces (D-F, orange, methyl groups): 3,5-dimethylphenylcarbamate (A, D), 4-methylphenylcarbamate (B, E), 2,5-dimethylphenylcarbamate (C, F). (For interpretation of the references to colour in this figure legend, the reader is referred to the Web version of this article.)

details see Table S2, Supplementary data). When two enantiomers could be at least partially resolved, the enantiomer elution order (EEO) was (*M*)-(*P*) in all cases, and no reversal of the elution sequence was observed as the CSP structure changed.

For compound **1**, high retention and selectivity were obtained with all chiral columns, except for the Cellulose-1 for which no enantioseparation was obtained. Compound **1** was enantioseparated with selectivity factors ranging from 2.01 to 5.08 by using i-Cellulose-5 and the three amylose-based chiral columns. Whereas **1** was eluted with moderate retention ($k = 1.96$) on Cellulose-1, on the other four columns the second eluted (*P*)-enantiomer showed higher retention factors, ranging from 7.46 to 31.60.

On the contrary, the enantioseparation of compound **2** was unsuccessful in most cases, and baseline enantioseparation was obtained with Cellulose-1 exclusively ($\alpha = 2.94$). Compound **2** remained unseparated with i-Cellulose-5, whereas amylose-based chiral columns provided enantioseparations featuring very low selectivity ($1.04 \leq \alpha \leq 1.10$) and moderate retention ($1.51 \leq k \leq 2.15$).

On one hand, the symmetry of the phenyl derivative **2** could be a reason for the low rate of baseline enantioseparation obtained for this compound. On the other hand, based on the chromatographic results, the selected chiral columns systematically showed reverse performances toward compounds **1** and **2**. For instance, complementary performances of Cellulose-1 vs i-Cellulose-5 and Amylose-1 towards the two analytes could be observed, namely as pendant groups and backbone structures changed, respectively (Fig. S1, Supplementary data). Whereas compound **2** was baseline enantioseparated on the Cellulose-1 but not on i-Cellulose-5 and Amylose-1, the opposite could be observed for compound **1**. Interestingly, with the i-Cellulose-5, and more with the Amylose-1, the most retained (*P*)-**1** enantiomer showed very high affinity toward the selectors, with retention times of 51.77 min and 111.36 min, respectively. Given the higher electrophilic character of the amidic hydrogen of the dichlorinated selector compared to the dimethylated polymer, it was unlikely that the high retention observed for compound **1** on both columns was primarily due to HBs involving the nucleophilic moieties of the ferrocenyl derivative, namely the pyridyl nitrogens and the ethynyl π-electron clouds. Indeed, for an HB-driven enantioseparation higher retention and selectivity could be expected for the i-Cellulose-5 compared to Amylose-1, whereas the opposite was observed. Furthermore, the effect of introducing chlorine in the selector appeared dependent on both analyte and selector backbone structures (α (**1**): i-Cellulose-5 > Cellulose-1 and i-Amylose-3 < Amylose-1/i-Amylose-1; α (**2**): i-Cellulose-5 < Cellulose-1 and i-Amylose-3 > Amylose-1/i-Amylose-1). By comparing the chromatographic performances of Amylose-1 and i-Amylose-1, the impact of immobilization on the enantioseparation could be evaluated. Again, it could be observed that the selectivity of compound **1** decreased (from 5.08 to 2.02, −60.2%) and that of compound **2** increased (from 1.04 to 1.07, +2.9%), by changing the coated amylose-based column to its immobilized version. Thus, it was likely that, besides HBs, other interactions related to the extended π-electron system could contribute to analyte adsorption and enantiorecognition.

Given these experimental results, with the aim to determine and compare the contribution of van der Waals forces to the interaction energy (E_{int}) of ferrocene and benzene with the amylose *tris*(3,5-dimethylphenylcarbamate), a 100 ns MD simulation was performed by using a nonamer of the amylose-based polymer, benzene and ferrocene as guests, and the mixture *n*-hexane/2-PrOH 90:10 as explicit solvent. The E_{int} between the aromatic guests and the nonamer was calculated based on the energies of the nonamer-aromatic guest complex, the nonamer, and the aromatic guest (Eq. (2)):

$$E_{int} = E_{total} - E_{guest} - E_{amylose-based\ nonamer} \quad (2)$$

where the E_{int} term is derived from the contributions of the van der Waals (vdW) and the electrostatic (el) interaction terms (Eq. (3)):

$$E_{int} = E_{el} + E_{vdW} \quad (3)$$

In this regard, it is worth mentioning that most popular force fields include dispersion interactions through the Lennard-Jones potential (Eq. (4)) [48]:

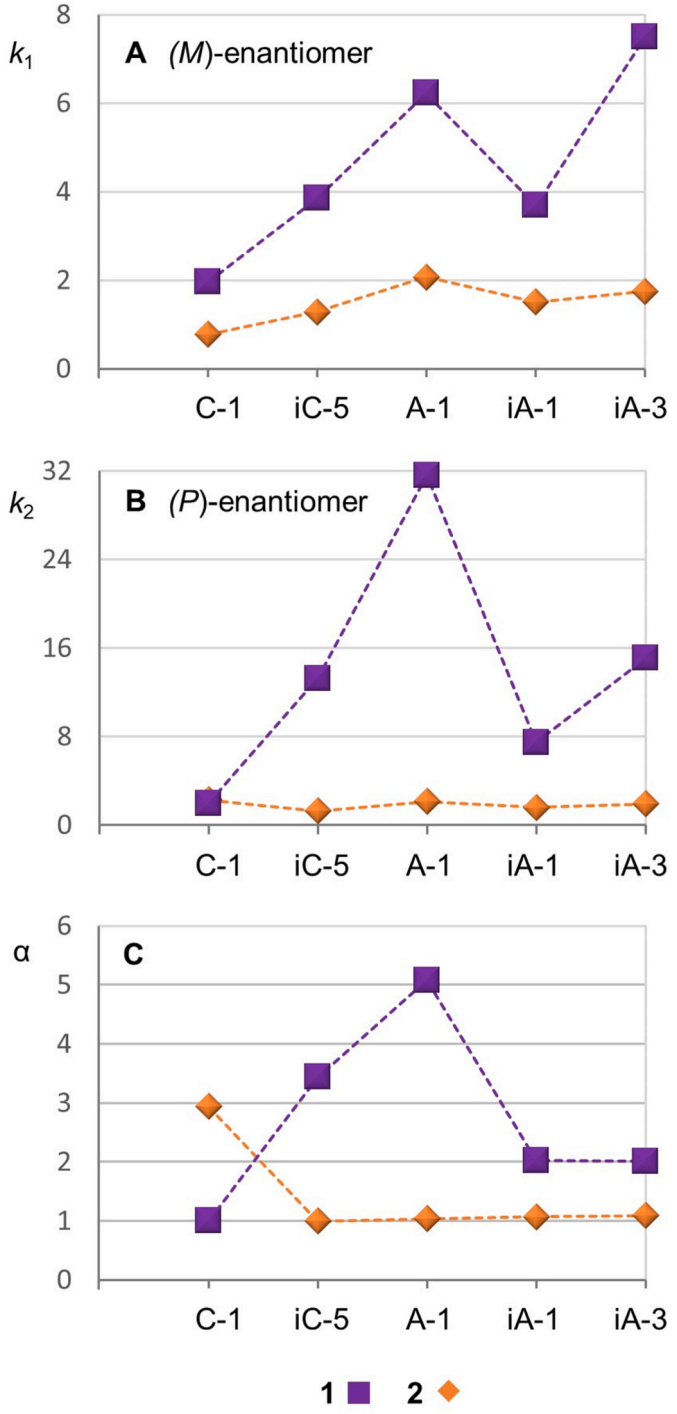

Fig. 3. Comparison of retention factors of first (k_1) (*M*) and of second (k_2) (*P*) eluted enantiomers, and selectivity (α) of compounds **1** and **2** on Lux Cellulose-1 (C-1), i-Cellulose-5 (iC-5), Amylose-1 (A-1), i-Amylose-1 (iA-1), and i-Amylose-3 (iA-3) as chiral columns with *n*-hexane/2-PrOH 90:10 v/v as mobile phase (flow rate = 0.8 ml/min, T = 25 °C) (for chromatographic parameters see Table S2, Supplementary Data).

$$E_{LJ,ij}(r_{ij}) = \frac{A_{ij}}{r_{ij}^{12}} - \frac{C_{6,ij}}{r_{ij}^{6}} \quad (4)$$

where the A/r^{12} term of this equation represents Pauli repulsion, whereas dispersion interactions are represented by the C_6/r^6 term.

On this basis, a higher contribution of the E_{vdW} and a lower contribution of the E_{el} to E_{int} was determined for ferrocene (81.3% for E_{vdW}; 18.7% for E_{el}) compared to benzene (77.8% for E_{vdW}; 22.2% for E_{el})

Table 2
Interaction energies (E_{int}) (kcal·mol^{-1}) and component contributions (E_{el}, E_{vdW}) for the association of benzene and ferrocene with the nonamer of amylose *tris* (3,5-dimethylphenylcarbamate) (solvent box *n*-hexane/2-PrOH 90:10), as derived from MD trajectories.

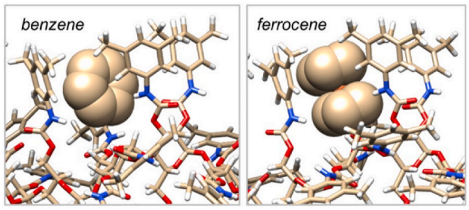

Compound	E_{int}	E_{el}	E_{vdW}
benzene	−16.23	−3.60	−12.63
ferrocene	−18.89	−3.53	−15.36

(Table 2), confirming the higher ability of the ferrocene moiety as dispersion energy fragment. In addition, it is interesting to note that although amylose-based derivatives are more sensitive to the steric hindrance of the chiral analytes because they have a more compact structure compared to cellulose-based polymers [49], ferrocene appeared to penetrate better in the chiral cavity, likely due to more close contact with the amylose backbone surface.

3.6. Impact of mobile phase polarity on the enantioseparation of compounds 1 and 2

With the aim to increase the contribution of π-cloud-based interactions in the enantioseparation of compounds **1** and **2**, the intramolecular HBs potentially contributing to enantioseparation were weakened by using more polar MeOH-containing mobile phases. Given that, *n*-hexane/2-PrOH/MeOH 90:5:5 v/v/v was used as mobile phase

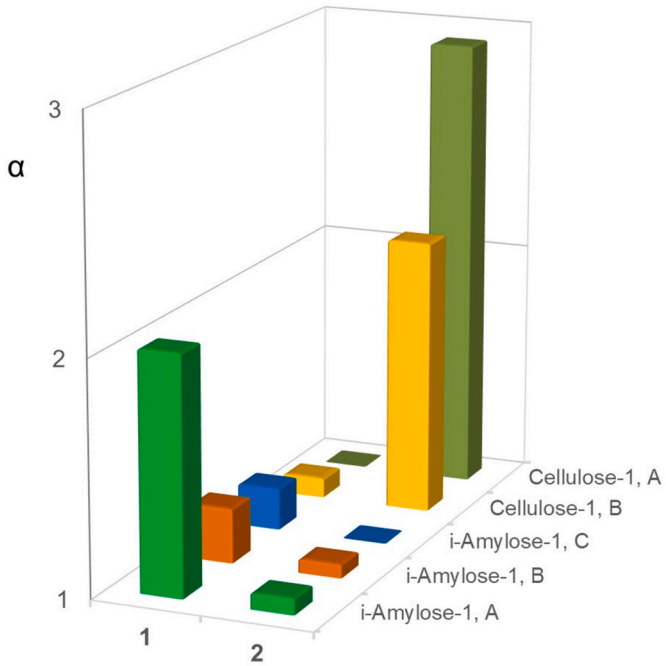

Fig. 4. Comparison of selectivity factor (α) of compounds **1** and **2** on Lux Cellulose-1 and i-Amylose-1 with *n*-hexane/2-PrOH 90:10 v/v (A), *n*-hexane/2-PrOH/MeOH 90:5:5 v/v/v (B), and pure MeOH (C) as mobile phases (flow rate = 0.8 ml/min, T = 25 °C) (for chromatographic parameters see Table S3, Supplementary Data).

with Cellulose-1 and i-Amylose-1, whereas pure MeOH as mobile phase was also considered with the immobilized amylose-based chiral column (Fig. 4 and Table S3, Supplementary data). The EEO remained (*M*)-(*P*) for both compounds in all cases, thus no reversal of elution sequence was observed for this series of enantioseparations.

On Cellulose-1, the introduction of 5% MeOH in the mobile phase, changing the binary mixture *n*-hexane/2-PrOH 90:10 v/v to the ternary *n*-hexane/2-PrOH/MeOH 90:5:5 v/v/v, had the effect of decreasing the selectivity for compound **2** (from 2.94 to 2.18) given that the retention factor of the first and the second eluted enantiomers increased (from 0.78 to 0.93) and decreased (from 2.29 to 2.04), respectively. Despite that, baseline enantioseparation was again obtained in this case. The opposite trend was observed for compound **1**, and with the MeOH-containing ternary mixture, the selectivity slightly increased from 1.00 to 1.08. Under these conditions, the ferrocenyl derivative was partially resolved, whereas retention factors decreased for both enantiomers (from 1.96 to 1.68 and 1.82). On this basis, the effect of mobile phase polarity on the enantioseparation of compounds **1** and **2** with the Cellulose-1 depended on the distinctive analyte structure.

On i-Amylose-1, the effect of introducing 5% MeOH in the mobile phase provided opposite enantioseparation outcomes for compound **1** compared to Cellulose-1. Indeed, baseline enantioseparation was also obtained with the MeOH-containing mixture, but selectivity decreased (from 2.02 to 1.24) mainly due to the significant decrease of retention factor of the most retained (*P*)-**1** enantiomer (from 7.36 to 3.15). Using pure MeOH as mobile phase, selectivity decreased further to 1.18 and **1** was only partially resolved under these elution conditions. The enantioseparation of compound **2** remained almost unchanged by adding 5% MeOH in the mobile phase (α changing from 1.07 to 1.06), whereas the enantioseparation was totally suppressed by using pure MeOH as mobile phase.

This short screening proved that adding MeOH to mobile phase impacted differently adsorption and recognition mechanisms of **1** and **2** on Cellulose-1 and i-Amylose-1, in a manner dependent on analyte and backbone structure. For compound **1**, the most important changes on the i-Amylose-1 occurred at low concentration of MeOH (5%), with a percentage reduction of k_2 and α of 58% and 39%, respectively. On the other hand, changing the ternary mixture to pure MeOH had a lower impact on both k_2 and α with a percentage decrease of 11% and 5%. This means that the noncovalent interaction pattern underlying high retention and selectivity on the amylose-based columns was only sensitive to small amounts of MeOH added to the mobile phase, and that further addition of methanol did not significantly impact on the noncovalent interaction pattern. In mechanistic terms, two types of noncovalent interactions appeared to promote the enantioseparation of the bis-ferrocenyl derivatives, one sensitive to MeOH, likely HB, and a second interaction with the following features: *a*) persistent under polar organic elution conditions, *b*) occurring with the bis-ferrocenyl derivative exclusively, and *c*) able to positively cooperate with the HB providing high k_2 and large selectivity with MeOH-free mobile phases.

3.7. Effect of temperature on the enantioseparation

The chromatographic screening performed on analytes **1** and **2** showed that their extended π-electron clouds distinctively interacted with the selectors. Thus, to explore the nature of analyte/CSP association based on thermodynamic considerations, the approach based on van't Hoff plots was applied (see Supplementary data for theory details), and thermodynamic parameters were calculated for the analyte transfer from the liquid phase to the CSP. On one hand, criticisms have been reported in the literature about the use of this methodology to characterize retention mechanisms in chiral chromatography by determining enthalpy (ΔH°) and entropy (ΔS°) change for analyte adsorption [50,51]. In principle, deconvolution of the individual stereoselective and nonstereoselective interactions cannot be made by this procedure. On the other hand, it has been fully demonstrated that interesting and reasonably reliable information on chiral recognition mechanisms can be derived from van't Hoff plots when chemically related chiral analytes are treated, and their retention studied by systematically changing experimental conditions [52–54]. In these cases, a thermodynamic picture of different interaction patterns can be fruitfully derived and compared.

Based on these considerations, retention and selectivity of compounds **1** and **2** on the five chiral columns used in this study were determined at different temperatures from 5 to 45 °C in 5 °C increments by using *n*-hexane/2-PrOH 90:10 v/v as mobile phase (Table S4, Supplementary data). The thermodynamic quantities derived from van't Hoff plots (Fig. 5 and Fig. S2, Supplementary data) are reported in Table S5. The following remarks emerged from the thermodynamics study.

i) Compounds **1** and **2** showed different thermodynamics profiles on all columns, and the temperature-dependence pattern was observed to be a function of the 5,5′-aromatic substituents (Fig. 5).

ii) With Cellulose-1, compound **1** could be partially resolved below 20 °C. On the contrary, compound **2** could be partially resolved above 20 °C with Amylose-1, whereas it remained unresolved over the entire temperature 5–45 °C range on i-Cellulose-5.

iii) For compound **1**, enantioseparation was enthalpy-driven on all columns. On the contrary, enantioseparation of compound **2** was entropy-driven on both Amylose-1 (T_{iso} = 8 °C; Q = 0.94) and i-Amylose-1 (T_{iso} = −31 °C; Q = 0.81), whereas enthalpy-driven thermodynamics were derived for the enantioseparation with the Cellulose-1 and i-Amylose-3. No EEO reversal was observed for compound **2**, and (*M*)-(*P*) was the elution sequence at all examined temperature. It is worth noting that although reversal of EEO was expected with the Amylose-1 below T_{iso} (8 °C), compound **2** remained not separated at 5 °C. On the other hand, co-elution is often observed in a certain temperature range around the T_{iso} [52] due to finite peak width in chromatography.

iv) The evaluation of the variations of the ΔH and ΔS values, determined for the adsorption of each enantiomer on the selector surface as the chiral selectors changed, showed two distinctive fingerprints for each compound (Fig. S3, Supplementary data). For both enantiomers of compound **1**, the most negative ΔH (−4463.82 and −10869.37 cal·mol^{-1}) and ΔS (−12.25 and −31.29 cal·mol^{-1}·K^{-1}) values were observed on the i-Cellulose-5, likely due to the HBs involving the highly electrophilic carbamate amidic moieties of the dichlorinated chiral selector. On the other hand, both enantiomers of **1** were more retained on the Amylose-1 than on i-Cellulose-5 due to a lower entropy penalty featuring the adsorption thermodynamics on the amylose-based column (ΔS_1: 1.15 vs −12.25 cal·mol^{-1}·K^{-1}; ΔS_2: 7.98 vs −31.29 cal·mol^{-1}·K^{-1}). On the contrary, compound **2** showed the less negative ΔH and ΔS values on i-Cellulose-5, whereas the most negative values were determined for the methylchlorinated i-Amylose-3. This could confirm that HBs played a role in determining the affinity of the enantiomers toward the chiral selector, with the selector HB-ability being modulated by the backbone (amylose or cellulose) structural features.

v) For the enantioseparation of compound **1** on the Amylose-1 in the temperature range 5–45 °C, a lower temperature dependence of retention for the first eluted (*M*)-enantiomer compared to the second eluted (*P*)-enantiomer (Fig. 6) was observed. In addition, the (*P*)-enantiomer peak appeared significantly broader compared to that of the first eluted enantiomer. In terms of thermodynamics parameters, the van't Hoff analysis also showed a substantial difference in ΔH (−1423.69 vs −4413.09 cal·mol^{-1}) and in ΔS (−1.15 vs −7.98 cal·mol^{-1}·K^{-1}) values for the adsorption of the two enantiomers on the Amylose-1. A similar trend was also observed for the enantioseparation of **1** with the i-

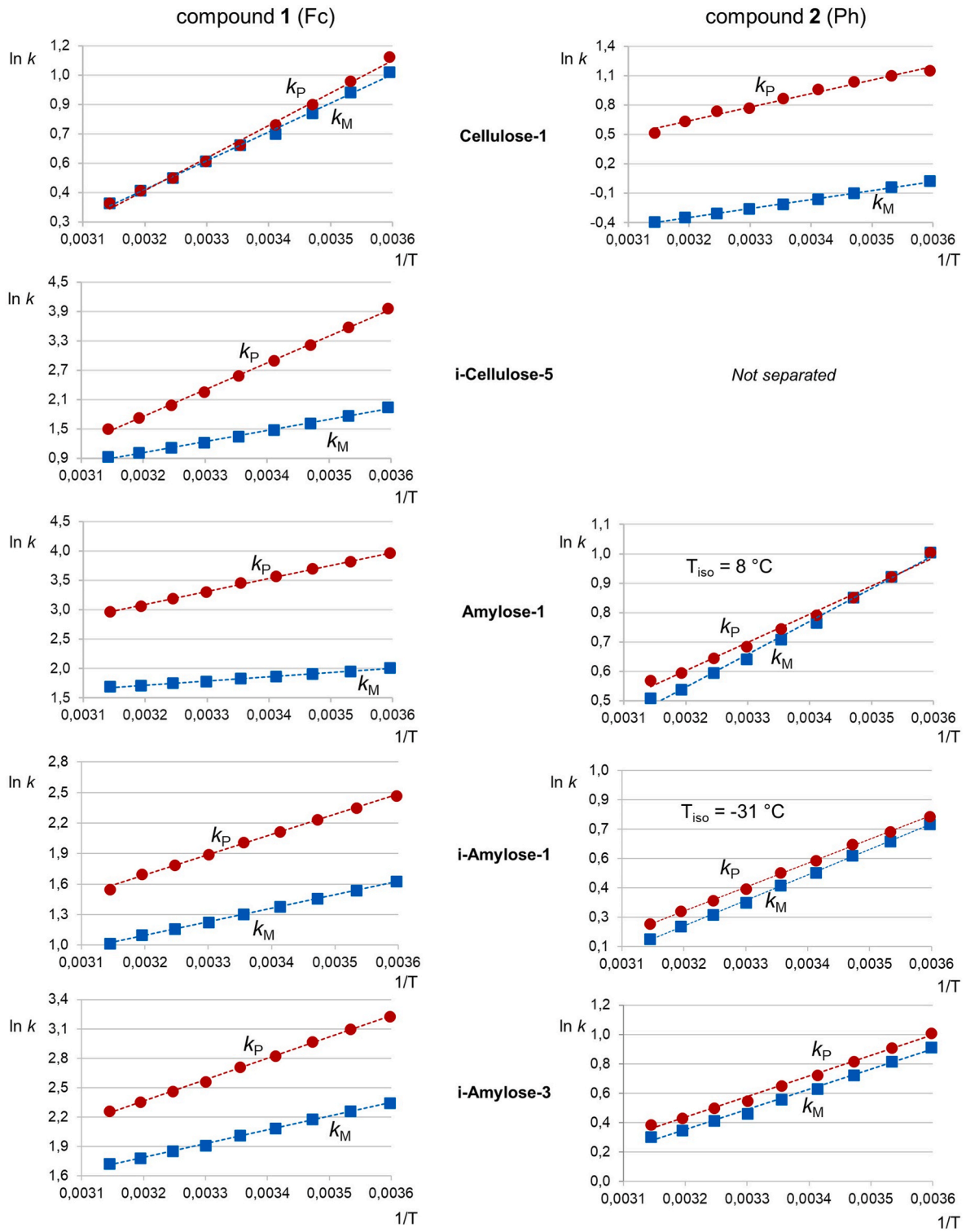

Fig. 5. Ln *k* vs. 1/T van't Hoff plots for the enantioseparation of **1** and **2** on Lux Cellulose-1, i-Cellulose-5, Amylose-1, i-Amylose-1, and i-Amylose-3 (*n*-hexane/2-PrOH 90:10, 0.8 ml/min, temperature range 278.15–318.15 K) (for chromatographic parameters see Table S4, Supplementary Data).

Cellulose-5 (ΔH: 4463.82 vs −10869.37 cal·mol^{-1}; ΔS: 12.25 vs −31.29 cal·mol^{-1}·K^{-1}). In both cases, at 5 °C, the (*P*)-enantiomer was eluted with similar retention times close to 200 min. On the contrary, at 45 °C i-Cellulose-5 provided lower retention factors for **1** compared to Amylose-1, showing that, likely, temperature-sensitive interactions, like HB, were weakened or even suppressed at higher temperature on the chlorinated selector. Despite the similarity of the chromatographic traces, the results accounting for enantioseparation thermodynamics of **1** on Amylose-1 and i-Cellulose-5 suggested two distinctive mechanisms for the adsorption of each enantiomer on the selector surfaces, and the presence of strong noncovalent interactions (other than HBs) underlying the adsorption of the most retained (*P*)-enantiomer.

vi) Through the van't Hoff plots, the differences in the enthalpy and entropy of adsorption on the stationary phase, $\Delta\Delta H$ and $\Delta\Delta S$,

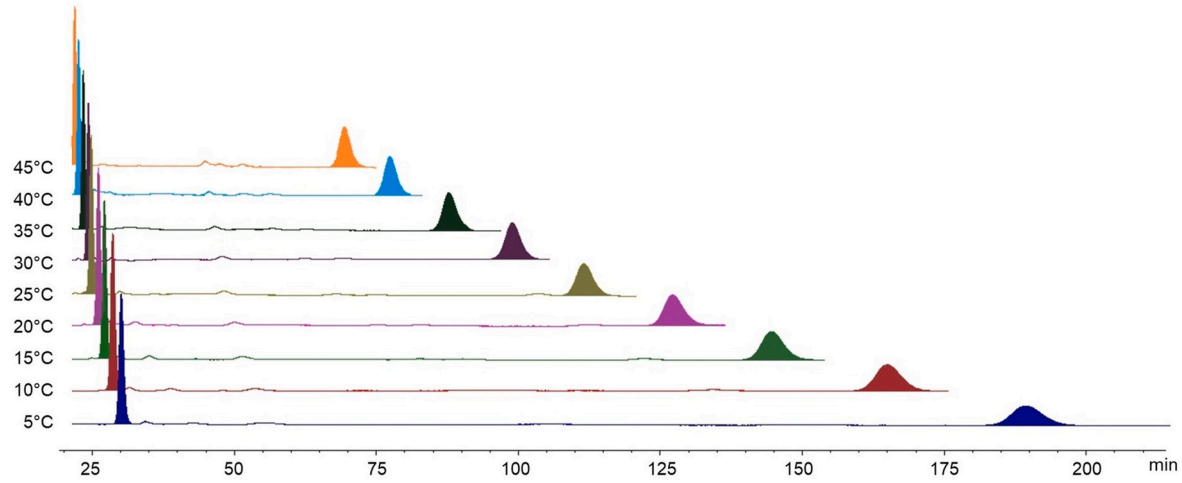

Fig. 6. Effect of temperature on the enantioselectivity of compound **1** (Lux Amylose-1, *n*-hexane/2-PrOH 90:10 v/v, 0.8 ml/min) (for chromatographic parameters see Table S4, Supplementary Data).

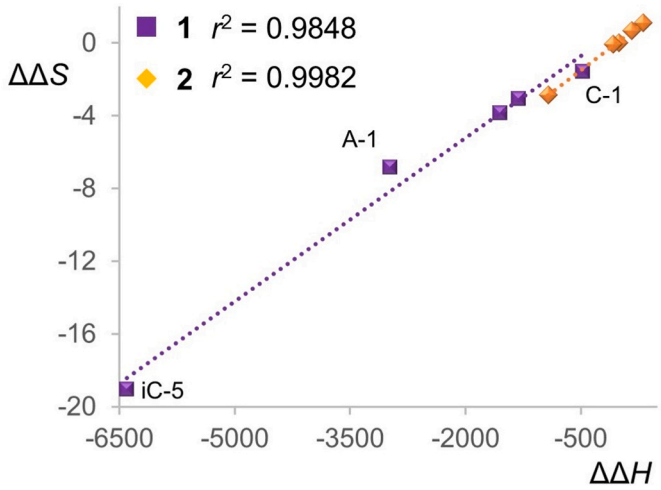

Fig. 7. Enthalpy-entropy (ΔΔ*H*, cal·mol^{-1}) (ΔΔ*S*, cal·mol^{-1}·K^{-1}) compensation for **1** and **2** on Lux Cellulose-1, i-Cellulose-5, Amylose-1, i-Amylose-1, and i-Amylose-3 (*n*-hexane/2-PrOH 90:10, 0.8 ml/min, temperature range 278.15–318.15 K) (for chromatographic parameters see Table S5, Supplementary Data).

respectively, were determined. Fig. 7 shows the entropy-enthalpy compensation graphs for compounds **1** and **2.** In both cases, the regression lines exhibited a linear trend (r^2 = 0.9848 (**1**), 0.9982 (**2**)) because of the balance between the thermodynamic quantities. The data set profiles two different lines for each compound, that of the bis-ferrocenyl derivatives slightly shifted toward less negative ΔΔ*S* values. It is interesting to note that the linearity of the enthalpy–entropy compensation graph including *n* operative enantioseparation conditions is considered consistent with an interaction mode which is shared by the *n* enantioseparations. On this basis, the comparison of the two straight lines confirmed that two distinctive interaction modes featured the enantioseparation of the two analytes in most cases. In addition, a slight break in linearity could be observed for the enantioseparation of **1** on Amylose-1, confirming that noncovalent interactions other than the main interaction mode occurred with this chiral column. Interestingly, the point representing the thermodynamic data determined for the enantioseparation of **1** on the Cellulose-1 lay on the straight line profiling the thermodynamics of compound **2.** This observation may suggest that on the cellulose-based column the two analytes shared the same interaction mode which, however, resulted in a successful enantioseparation for the bis-phenyl derivative **2** exclusively.

vii) Column immobilization (Amylose-1 vs i-Amylose-1) provided different effects on the enantioseparation of the two analytes. For compound **1**, moving from coated to immobilized selector, affinity of the first (*M*)- and the second eluted (*P*)-enantiomers increased and decreased, respectively, resulting in reduced enantioselective recognition (ΔΔ*G*° changed from −953.02 to −411.08 cal·mol^{-1}). In this regard, it is worth mentioning that immobilization decreases the selector surface exposed to the analyte and this feature is expected to be detrimental for a dispersion-driven binding mechanism. For compound **2**, by changing Amylose-1 to i-Amylose-1, the thermodynamic affinity of both enantiomers increased producing a slight increase of selectivity (ΔΔ*G*° changed from −19.04 to −38.82 cal·mol^{-1}).

4. Conclusions

In this study, the enantioseparation of bis-ferrocenyl 4,4′-bipyridine **1** was explored and compared to that of bis-phenyl derivative **2** with the aim to evaluate the potential contribution of dispersion forces to the enantioseparation of the ferrocenyl-containing analyte. For this purpose, five chiral columns based on amylose and cellulose *tris*(3,5-disubstitutedphenylcarbamates) were used as chiral selectors, with *n*-hexane-based mixtures as mobile phases. In most cases, the enantioseparability of compound **2** was low due to the inherent symmetry of the compound as well as to the lower electron charge density distribution on the main recognition sites. Significantly large enantioseparations were obtained for the bis-ferrocenyl derivative **1** on the Amylose-1 and the i-Cellulose-5, with differences likely depending on the strength of HBs acting in cooperation with forces involving the extended π-electron system of the analyte. Despite its large-sized structure, the *P*-enantiomer of the bis-ferrocenyl analyte showed high affinity for the compact amylose-based selector. Under the same elution conditions, the bis-phenyl derivative **2** remained unresolved or provided poor selectivity. In this regard, MD simulations proved the higher ability of ferrocene to penetrate into the groove of the amylose-based polymer compared to benzene, this process being mainly driven by van der Waals interactions. In addition, the two analytes showed different thermodynamic profiles with both coated and immobilized amylose *tris*(3,5-dimethylphenylcarbamate)-based chiral columns, enthalpy-driven for the bis-ferrocenyl derivative and entropy-driven for the bis-phenyl-substituted analyte. Thus, experimental and theoretical analyses reasonably

supported the following conclusions: *a*) despite the structural similarity of the analytes, the enantioselective recognition of compounds **1** and **2** on the selected CSPs was driven by different mechanisms and non-covalent interaction patterns and, consequently, *b*) the involvement of the distinctive extended π-electron clouds in the interaction with the selector surface was different for each of the two analytes. As a result, mechanisms and noncovalent interactions underlying successfully enantiorecognition for the bis-ferrocenyl derivative appeared detrimental for the enantioseparation of the bis-phenyl compound, and *vice versa*.

Dispersion forces are subtle interactions, not easy to detect and to identify neither experimentally nor theoretically; thus, focused theoretical analyses are needed to conclusively confirm that dispersion forces based on induced dipole formation may contribute to analyte-selector interactions and to enantioselective recognition with polysaccharide-based selectors. Despite that, this study demonstrated that different mechanisms and noncovalent interaction patterns underlie adsorption and enantioselective recognition of the structurally related analytes **1** and **2** depending on the peculiar steric and electronic properties of the cylindrical ferrocene compared to the flat benzene as distinctive substituents. The reported data are reasonably consistent with a picture of the enantioselective recognition based on the interplay between HBs, π-π stacking and dispersion interactions dependent on analyte structure and features of the polysaccharide surfaces.

CRediT authorship contribution statement

Barbara Sechi: Formal analysis, HPLC analysis, Data curation, Writing – review & editing. **Alessandro Dessì:** Formal analysis, Writing – review & editing. **Roberto Dallocchio:** Formal analysis, Writing – review & editing. **Nutsa Tsetskhladze:** Data curation, Writing – review & editing. **Bezhan Chankvetadze:** Resources, Writing – review & editing. **Mireia Pérez-Baeza:** Formal analysis, HPLC analysis, Data curation, Writing – review & editing. **Sergio Cossu:** Data curation, Writing – review & editing. **Giorgi Jibuti:** Data curation, Writing – review & editing. **Victor Mamane:** Project administration, Syntheses, Funding acquisition, Writing – review & editing. **Paola Peluso:** Conceptualization, Project administration, Funding acquisition, Methodology, Formal analysis, Writing – original draft, Writing – review & editing, review & editing.

Declaration of competing interest

The authors declare that they have no known competing financial interests or personal relationships that could have appeared to influence the work reported in this paper.

Data availability

Data will be made available on request.

Acknowledgements

Open Access funding provided by Consiglio Nazionale delle Ricerche (CNR) within the CRUI-CARE agreement. We also thank CNR (Grant no.: SAC.AD002.011.032) and SRNSFG (Shota Rustaveli National Science Foundation of Georgia) (Grant no.: CNR-19-075) for the Italy-Georgia Joint Bilateral Agreement, and the University of Strasbourg, the Centre National de la Recherche Scientifique (CNRS), and the French National Research Agency (Grant no.: ANR-21-CE07-0014) for financial support.

Appendix A. Supplementary data

Supplementary data to this article can be found online at https://doi.org/10.1016/j.aca.2023.341725.

References

[1] B. Chankvetadze, Recent trends in preparation, investigation and application of polysaccharide-based chiral stationary phases for separation of enantiomers in high-performance liquid chromatography, Trends Anal. Chem. 122 (2020), 115709, https://doi.org/10.1016/j.trac.2019.115709.
[2] P. Peluso, V. Mamane, R. Dallocchio, A. Dessì, S. Cossu, Noncovalent interactions in high-performance liquid chromatography enantioseparations on polysaccharide-based chiral selectors, J. Chromatogr. A 1623 (2020), 461202, https://doi.org/10.1016/j.chroma.2020.461202.
[3] B. Chankvetadze, Recent developments on polysaccharide-based chiral stationary phases for liquid-phase separation of enantiomers, J. Chromatogr. A 1269 (2012) 26–51, https://doi.org/10.1016/j.chroma.2012.10.033.
[4] P. Peluso, B. Chankvetadze, The molecular bases of chiral recognition in 2-(benzylsulfinyl)benzamide enantioseparation, Anal. Chim. Acta 1141 (2021) 194–205, https://doi.org/10.1016/j.aca.2020.10.050.
[5] P. Peluso, V. Mamane, A. Dessì, R. Dallocchio, E. Aubert, C. Gatti, D. Mangelings, S. Cossu, Halogen bond in separation science: a critical analysis across experimental and theoretical results, J. Chromatogr. A 1616 (2020), 460788, https://doi.org/10.1016/j.chroma.2019.460788.
[6] P. Peluso, A. Dessì, R. Dallocchio, B. Sechi, C. Gatti, B. Chankvetadze, V. Mamane, R. Weiss, P. Pale, E. Aubert, S. Cossu, Enantioseparation of 5,5'-dibromo-2,2'-dichloro-3-selanyl-4,4'-bipyridines on polysaccharide-based chiral stationary phases: exploring chalcogen bonds in liquid-phase chromatography, Molecules 26 (2021) 221, https://doi.org/10.3390/molecules26010221.
[7] X. Aniban, B. Hartwig, A. Wuttke, R.A. Mata, Dispersion forces in chirality recognition – a density functional and wave function theory study of diols, Phys. Chem. Chem. Phys. 23 (2021) 12093–12104, https://doi.org/10.1039/D1CP01225H.
[8] M. Delle Piane, M. Corno, P. Ugliengo, Does dispersion dominate over H-bonds in drug−surface interactions? The case of silica-based materials as excipients and drug-delivery agents, J. Chem. Theor. Comput. 9 (2013) 2404–2415, https://doi.org/10.1021/ct400073s.
[9] S. Grimme, R. Huenerbein, S. Ehrlich, On the importance of the dispersion energy for the thermodynamic stability of molecules, ChemPhysChem 12 (2011) 1258–1261, https://doi.org/10.1002/cphc.201100127.
[10] D.C. Fang, S.C. Liu, D.Y. Liu, X.R. Zhu, The treatment of dispersion terms for solution systems, Phys. Chem. Chem. Phys. 25 (2023) 19422–19426, https://doi.org/10.1039/D3CP02733C.
[11] V. Mamane, E. Aubert, P. Peluso, S. Cossu, Synthesis, resolution, and absolute configuration of chiral 4,4'-bipyridines, J. Org. Chem. 77 (2012) 2579–2583, https://doi.org/10.1021/jo300286z.
[12] H. Koller, K.E. Rimböck, A. Mannschreck, High-pressure liquid chromatography on triacetylcellulose: characterization of a sorbent for the separation of enantiomers, J. Chromatogr. A 282 (1983) 89–94, https://doi.org/10.1016/S0021-9673(00)91594-2.
[13] M.J. Frisch, G.W. Trucks, H.B. Schlegel, G.E. Scuseria, M.A. Robb, J.R. Cheeseman, G. Scalmani, V. Barone, B. Mennucci, G.A. Petersson, H. Nakatsuji, M. Caricato, X. Hratchian, H.P. Li, A.F. Izmaylov, J. Bloino, G. Zheng, J.L. Sonnenberg, M. Hada, M. Ehara, K. Toyota, R. Fukuda, J. Hasegawa, M. Ishida, T. Nakajima, Y. Honda, O. Kitao, H. Nakai, T. Vreven, J.A. Montgomery Jr., J.E. Peralta, F. Ogliaro, M. Bearpark, J.J. Heyd, E. Brothers, K.N. Kudin, V.N. Staroverov, T. Keith, R. Kobayashi, J. Normand, K. Raghavachari, A. Rendell, J.C. Burant, S.S. Iyengar, J. Tomasi, M. Cossi, N. Rega, J.M. Millam, M. Klene, J.E. Knox, J.B. Cross, V. Bakken, C. Adamo, J. Jaramillo, R. Gomperts, R.E. Stratmann, O. Yazyev, A. J. Austin, R. Cammi, C. Pomelli, J.W. Ochterski, R.L. Martin, K. Morokuma, V. G. Zakrzewski, G. Voth, P. Salvador, J.J. Dannenberg, S. Dapprich, A.D. Daniels, O. Farkas, J.B. Foresman, J. Ortiz, J. Cioslowski, D.J. Fox, Gaussian 09, Revision B. 01, Inc.Gaussian, C.T, Wallingford, 2010.
[14] T. Lu, F. Chen, Multiwfn: a multifunctional wavefunction analyser, J. Comput. Chem. 33 (2012) 580–592, https://doi.org/10.1002/jcc.22885.
[15] T. Lu, F. Chen, Quantitative analysis of molecular surface based on improved Marching Tetrahedra algorithm, J. Mol. Graph. Model. 38 (2012) 314–323, https://doi.org/10.1016/j.jmgm.2012.07.004.
[16] IUPAC Gold Book, IUPAC compendium of chemical terminology – the gold book. https://goldbook.iupac.org/terms/view/L03617. (Accessed 26 April 2023).
[17] J.P. Wagner, P.R. Schreiner, London dispersion in molecular chemistry – reconsidering steric effects, Angew. Chem. Int. Ed. 54 (2015) 12274–12296, https://doi.org/10.1002/anie.201503476.
[18] S. Grimme, Dispersion interaction and chemical bonding, in: G. Frenking, S. Shaik (Eds.), The Chemical Bond - Chemical Bonding across the Periodic Table, John Wiley and Sons, Weinheim, 2014, pp. 477–478.
[19] F. Pinto, Dispersion force engineering. The long path from hooked atoms to next-generation spacecraft, Mater. Today: Proc. 54 (2022) 35–43, https://doi.org/10.1016/j.matpr.2021.09.135.
[20] G. Gryn'ova, C. Corminboeuf, Steric "attraction": not by dispersion alone, Beilstein J. Org. Chem. 14 (2018) 1482–1490, https://doi.org/10.3762/bjoc.14.125.
[21] L. Yang, C. Adam, G.S. Nichol, S.L. Cockroft, How much do van der Waals dispersion forces contribute to molecular recognition in solution? Nat. Chem. 5 (2013) 1006–1010, https://doi.org/10.1038/nchem.1779.
[22] M.A. Strauss, H.A. Wegner, London dispersion in alkane solvents, Angew. Chem. Int. Ed. 60 (2021) 779–786, https://doi.org/10.1002/anie.202012094.
[23] J.M. Schümann, J.P. Wagner, A.K. Eckhardt, H. Quanz, P.R. Shreiner, Intramolecular London dispersion interactions do not cancel in solution, J. Am. Chem. Soc. 143 (2021) 41–45, https://doi.org/10.1021/jacs.0c09597.

[24] C. Eschmann, L. Song, P.R. Schreiner, London dispersion interactions rather than steric hindrance determine the enantioselectivity of the Corey–Bakshi–Shibata reduction, Angew. Chem. Int. Ed. 60 (2021) 4823–4832, https://doi.org/10.1002/anie.202012760.
[25] D. Yepes, F. Neese, B. List, G. Bistoni, Unveiling the delicate balance of steric and dispersion interactions in organocatalysis using high-level computational methods, J. Am. Chem. Soc. 142 (2020) 3613–3625, https://doi.org/10.1021/jacs.9b13725.
[26] R.P.W. Scott, The role of molecular interactions in chromatography, J. Chromatogr. A 122 (1976) 35–53, https://doi.org/10.1016/S0021-9673(00)82235-9.
[27] M. Turowski, T. Morimoto, K. Kimata, H. Monde, T. Ikegami, K. Hosoya, N. Tanaka, Selectivity of stationary phases in reversed-phase liquid chromatography based on the dispersion interactions, J. Chromatogr. A 911 (2001) 177–190, https://doi.org/10.1016/S0021-9673(00)01193-6.
[28] R.K. Lindsey, J.L. Rafferty, B.L. Eggimann, J.I. Siepmann, M.R. Schure, Molecular simulation studies of reversed-phase liquid chromatography, J. Chromatogr. A 1287 (2013) 60–82, https://doi.org/10.1016/j.chroma.2013.02.040.
[29] T. Kubo, E. Kanao, T. Matsumoto, T. Naito, T. Sano, M. Yan, K. Otsuka, Specific intermolecular interactions by the localized π-electrons in C_{70}-fullerene, ChemistrySelect 1 (2016) 5900–5904, https://doi.org/10.1002/slct.201601470.
[30] H. Kobayashi, K. Okada, S. Tokuda, E. Kanao, Y. Masuda, T. Naito, H. Takaya, M. Yan, T. Kubo, K. Otsuka, Separation of saccharides using fullerene-bonded silica monolithic columns via π interactions in liquid chromatography, Sci. Rep. 10 (2020), 13850, https://doi.org/10.1038/s41598-020-70904-3.
[31] C. West, G. Guenegou, Y. Zhang, L. Morin-Allory, Insights into chiral recognition mechanisms in supercritical fluid chromatography. II. Factors contributing to enantiomer separation on tris-(3,5-dimethylphenylcarbamate) of amylose and cellulose stationary phases, J. Chromatogr. A 1218 (2011) 2033–2057, https://doi.org/10.1016/j.chroma.2010.11.085.
[32] S. Khater, Y. Zhang, C. West, Insights into chiral recognition mechanism in supercritical fluid chromatography III. Non-halogenated polysaccharide stationary phase, J. Chromatogr. A 1363 (2014) 278–293, https://doi.org/10.1016/j.chroma.2014.06.084.
[33] P. Peluso, V. Mamane, E. Aubert, S. Cossu, Insights into the impact of shape and electronic properties on the enantioseparation of polyhalogenated 4,4'-bipyridines on polysaccharide-type selectors. Evidence of stereoselective halogen bonding interactions, J. Chromatogr. A 1345 (2014) 182–192, https://doi.org/10.1016/j.chroma.2014.04.040.
[34] C. Park, J. Almlöf, The electronic and molecular structure of ferrocene, J. Chem. Phys. 95 (1991) 1829–1833, https://doi.org/10.1063/1.461031.
[35] A. Vargas-Caamal, S. Pan, F. Ortiz-Chi, J.L. Cabellos, R.A. Boto, J. Contreras-García, A. Restrepo, P.K. Chattaraj, G. Merino, How strong are the metallocene–metallocene interactions? Cases of ferrocene, ruthenocene, and osmocene, Phys. Chem. Chem. Phys. 18 (2016) 550–556, https://doi.org/10.1039/C5CP05956A.
[36] R.J. Durand, S. Achelle, S. Gauthier, N. Cabon, M. Ducamp, S. Kahlal, J.Y. Saillard, A. Barsella, F. Robin-Le Guena, Incorporation of a ferrocene unit in the π-conjugated structure of donor-linker-acceptor (D-π-A) chromophores for nonlinear optics (NLO), Dyes Pigments 155 (2018) 68–74, https://doi.org/10.1016/j.dyepig.2018.03.029.
[37] S. Grimme, Do special noncovalent π-π stacking interactions really exist? Angew. Chem. Int. Ed. 47 (2008) 3430–3434, https://doi.org/10.1002/anie.200705157.
[38] A. Patti, S. Pedotti, C. Sanfilippo, Comparative HPLC enantioseparation of ferrocenylalcohols on two cellulose-based chiral stationary phases, Chirality 19 (2007) 344–351, https://doi.org/10.1002/chir.20386.
[39] C. Gatti, A. Dessì, R. Dallocchio, V. Mamane, S. Cossu, R. Weiss, P. Pale, E. Aubert, P. Peluso, Factors impacting σ- and π-hole regions as revealed by the electrostatic potential and its source function reconstruction: the case of 4,4'-bipyridine derivatives, Molecules 25 (2020) 4409, https://doi.org/10.3390/molecules25194409.
[40] A. Morvan, C. Garnier, C. Furman, D. Speybrouck, E. Boulanger, A. Ghinet, E. Lipka, Separation of planar chiral ferrocenes by capillary electrokinetic chromatography and liquid chromatography, J. Chromatogr., A 1677 (2022), 463306, https://doi.org/10.1016/j.chroma.2022.463306.
[41] C. Cantatore, M. Korb, H. Lang, R. Cirilli, ON/OFF receptor-like enantioseparation of planar chiral 1, 2-ferrocenes on an amylose-based chiral stationary phase: the role played by 2-propanol, Anal. Chim. Acta 1211 (2022), 339880, https://doi.org/10.1016/j.aca.2022.339880.
[42] P. Peluso, V. Mamane, Ferrocene derivatives with planar chirality and their enantioseparation by liquid-phase techniques, Electrophoresis 44 (2023) 158–189, https://doi.org/10.1002/elps.202200148.
[43] S. Tribedi, K. Kitaura, T. Nakajima, R.B. Sunoj, On the question of steric repulsion versus noncovalent attractive interactions in chiral phosphoric acid catalyzed asymmetric reactions, Phys. Chem. Chem. Phys. 23 (2021) 18936–18950, https://doi.org/10.1039/D1CP02499J.
[44] K.L. Mears, P.P. Power, Beyond steric crowding: dispersion energy donor effects in large hydrocarbon ligands, Acc. Chem. Res. 55 (2022) 1337–1348, https://doi.org/10.1021/acs.accounts.2c00116.
[45] R. Dallocchio, A. Dessì, M. Solinas, A. Arras, S. Cossu, E. Aubert, V. Mamane, P. Peluso, Halogen bond in high-performance liquid chromatography enantioseparations: description, features and modelling, J. Chromatogr. A 1563 (2018) 71–81, https://doi.org/10.1016/j.chroma.2018.05.061.
[46] C. Yamamoto, E. Yashima, Y. Okamoto, Structural analysis of amylose tris(3,5-dimethylphenylcarbamate) by NMR relevant to its chiral recognition mechanism in HPLC, J. Am. Chem. Soc. 124 (2002) 12583–12589, https://doi.org/10.1021/ja020828g.
[47] X. Wang, C.J. Jameson, S. Murad, Modeling enantiomeric separations as an interfacial process using amylose tris(3,5-dimethylphenyl carbamate) (ADMPC) polymers coated on amorphous silica, Langmuir 36 (2020) 1113–1124, https://doi.org/10.1021/acs.langmuir.9b03248.
[48] J.E. Jones, On the determination of molecular fields. II. From the equation of state of a gas, Proc. R. Soc. London, A 106 (1924) 463–477, https://doi.org/10.1098/rspa.1924.0082.
[49] R.B. Kasat, N.H.L. Wang, E.I. Franses, Effects of backbone and side chain on the molecular environments of chiral cavities in polysaccharide-based biopolymers, Biomacromolecules 8 (2007) 1676–1685, https://doi.org/10.1021/bm070006h.
[50] L.D. Asnin, M.V. Stepanova, van't Hoff analysis in chiral chromatography, J. Separ. Sci. 41 (2018) 1–19, https://doi.org/10.1002/jssc.201701264.
[51] A. Sepsey, An Adventurous journey around the thermodynamics of liquid chromatography, LCGC North Am. 40 (2022) 584–586, https://doi.org/10.56530/lcgc.na.qk2090y9.
[52] I. Matarashvili, G. Kobidze, A. Chelidze, G. Dolidze, N. Beridze, G. Jibuti, T. Farkas, B. Chankvetadze, The effect of temperature on the separation of enantiomers with coated and covalently immobilized polysaccharide-based chiral stationary phases, J. Chromatogr. A 1599 (2019) 172–179, https://doi.org/10.1016/j.chroma.2019.04.024.
[53] D. Tanács, T. Orosz, Z. Szakonyi, T.M. Le, F. Fülöp, W. Lindner, I. Ilisz, A. Péter, High-performance liquid chromatographic enantioseparation of isopulegol-based ß-amino lactone and ß-amino amide analogs on polysaccharide-based chiral stationary phases focusing on the change of the enantiomer elution order, J. Chromatogr. A 1621 (2020), 461054, https://doi.org/10.1016/j.chroma.2020.461054.
[54] P. Peluso, B. Sechi, G. Lai, A. Dessì, R. Dallocchio, S. Cossu, E. Aubert, R. Weiss, P. Pale, V. Mamane, B. Chankvetadze, Comparative enantioseparation of chiral 4,4'-bipyridine derivatives on coated and immobilized amylose-based chiral stationary phases, J. Chromatogr. A 1625 (2020), 461303, https://doi.org/10.1016/j.chroma.2020.461303.